

Communication

Effect of Film Thickness on Microstructural and Magnetic Properties of Lithium Ferrite Films Prepared on Strontium Titanate (001) Substrates

Kun Liu ¹, Ruyi Zhang ², Lu Lu ^{3,*}, Jiankang Li ¹ and Songyou Zhang ¹

¹ School of Electronics and Information Engineering, Suzhou Vocational University, Suzhou 215104, China; 92107@jssvc.edu.cn (K.L.); ljk@jssvc.edu.cn (J.L.); 92207@jssvc.edu.cn (S.Z.)

² Ningbo Institute of Materials Technology and Engineering, Chinese Academy of Sciences, Ningbo 315201, China; zhangrui@nimte.ac.cn

³ Ji Hua Laboratory, Foshan 528200, China

* Correspondence: lulu@jihualab.ac.cn

Abstract: Epitaxial lithium ferrite (LiFe_5O_8) films with different thicknesses were successfully fabricated on strontium titanate (SrTiO_3) (001) substrates using the magnetron sputtering deposition technique. The microstructural and magnetic properties of the films were characterized by an advanced transmission electron microscope and a magnetic measurement device. It was found that the formation of structural defects can be influenced by the thickness of the film. In addition to misfit dislocations, orientation domains form in thinner films and twin boundaries appear in thicker films, respectively, contributing to the misfit strain relaxation in the heterosystem. The magnetic measurement showed that the thinner films have enhanced magnetization and a relatively lower coercive field compared with the thicker films containing antiferromagnetic twin boundaries. Our results provide a way of tuning the microstructure and magnetic properties of lithium ferrite films by changing the film thickness.

Keywords: lithium ferrite; film thickness; defects; magnetic properties; electron microscopy



Citation: Liu, K.; Zhang, R.; Lu, L.; Li, J.; Zhang, S. Effect of Film Thickness on Microstructural and Magnetic Properties of Lithium Ferrite Films Prepared on Strontium Titanate (001) Substrates. *Coatings* **2023**, *13*, 2097. <https://doi.org/10.3390/coatings13122097>

Academic Editor: Panos Pouloupoulos

Received: 15 November 2023

Revised: 8 December 2023

Accepted: 15 December 2023

Published: 17 December 2023



Copyright: © 2023 by the authors. Licensee MDPI, Basel, Switzerland. This article is an open access article distributed under the terms and conditions of the Creative Commons Attribution (CC BY) license (<https://creativecommons.org/licenses/by/4.0/>).

1. Introduction

Lithium ferrite (LiFe_5O_8) has drawn widespread attention from researchers because of its remarkable physical properties, such as high saturation magnetization, high Curie temperature, high electric resistivity, low loss at high frequencies, and good chemical and thermal stability [1,2], which give it potential for application in components of microwave devices and spintronics [3,4]. LiFe_5O_8 has the inverse spinel structure, where the tetrahedral sites are occupied by Fe^{3+} , and the octahedral sites are shared by Li^+ and the remaining Fe^{3+} in a ratio of 1:3 (denoted as $\text{Fe}[\text{Li}_{0.5}\text{Fe}_{1.5}]\text{O}_4$). The antiparallel-aligned magnetic spin between the Fe^{3+} distributed at tetrahedral sites and octahedral sites leads to a high magnetic moment of 2.5 μB per formula unit [1,5]. Compared to the bulk material, spinel thin films exhibit microstructural variations such as the presence of planar defects, which can alter the electrical and magnetic structures of the films [6,7]. Thus, research efforts concentrating on the growth, structure, properties, and applications of spinel thin films have proliferated over the last few decades [8–10].

Generally, during the film deposition process, many degrees of freedom can be used to modify the structural and physical properties of the film [11–14]. Among them, changing the film thickness is a common method to manipulate the strain state of the film [15,16]. Particularly, tuning strain states not only causes the formation of oriented domains [17,18], but also lead to a different density of the antiphase boundaries in spinel films [19,20], which influence the magnetic properties of the films consequently [21]. Moreover, enhanced magnetic moments are present in ultrathin films (e.g., nickel-ferrite

(NiFe₂O₄) and cobalt-ferrite (CoFe₂O₄) prepared on spinel-type magnesium aluminate (MgAl₂O₄) substrates [22–24]. In contrast, there are limited investigations on the microstructural characteristic and magnetic behavior of LiFe₅O₈ films with different thicknesses prepared on perovskite-type substrates that are widely used as substrates for growing functional films in device applications.

In the present work, the microstructural and magnetic properties of LiFe₅O₈ films with two different thicknesses prepared on SrTiO₃ substrates are investigated using aberration-corrected (scanning) transmission electron microscopy ((S)TEM) and a superconducting quantum interference device (SQUID). The twin boundaries (TBs), orientation domains, and interface dislocation in the films are determined by high-angle annular dark-field (HAADF) imaging. The magnetic properties of the films are characterized through magnetization measurement using a SQUID magnetometer, and the effects of film thickness and structural defects on the magnetic properties of the LiFe₅O₈ films are discussed. This investigation provides a way of changing the thickness to manipulate the microstructure and the magnetic properties of LiFe₅O₈ films, allowing them to adapt to diverse technological applications, e.g., electrodes for rechargeable lithium-ion batteries, various components in microwave devices, and magnetic insulators for spin filtering in spintronics [25–27].

2. Materials and Methods

The LiFe₅O₈ ceramic target was prepared through a standard solid-state reaction method with the initial reactants iron oxide (Fe₂O₃) and lithium carbonate (Li₂CO₃) (ratio 5:2). The purity of the initial reactants Fe₂O₃ and Li₂CO₃ was 99.9%. The initial reactants were mixed through wet ball milling for 6 h and calcined at 900 °C for 4 h in a Muffle furnace (from Hefei Kejing Group, Hefei, China) to obtain LiFe₅O₈ powders. The LiFe₅O₈ powders were pressed into a two-inch cylinder by a hydraulic machine, and were then sintered at 1050 °C for 4 h in the Muffle furnace. The LiFe₅O₈ films were deposited with a radio-frequency (RF) sputtering system without applying a magnetic field during deposition. The sputtering system was on-axis, meaning that the sputtering target directly faced the substrate. The samples were fixed at a distance of 10 cm from the target without rotating the samples. The LiFe₅O₈ films with different thicknesses were fabricated on single-crystalline SrTiO₃ (001) substrates at a substrate temperature of 800 °C to ensure better crystalline quality of thin films. The film thicknesses were controlled by the deposition durations and confirmed by X-ray reflectivity (XRR) measurements [10]. The working pressure was 0.5 mbar with a mixed ambient of Ar and O₂ at a ratio of 1:1. The RF power was set at 100 W. After deposition, all films were post-annealed at 400 mbar in a mixed Ar/O₂ atmosphere.

(S)TEM specimens were prepared through a focused ion beam (FIB) lift-out technique using an FEI Helios600i FIB/SEM system. The Pt capping layer was deposited on the LiFe₅O₈ film to reduce ion beam damage and enhance the conductivity during preparation. FIB lamellae were cut along the <110> orientations of the SrTiO₃ substrate, and then, milled by 30 kV, 5 kV, and 1 kV Ga ion beams in sequence [20]. TEM and HAADF-STEM experiments were performed on a JEOL-ARM200F (JEOL Ltd., Tokyo, Japan) with a probe aberration corrector, operated at 200 kV. In STEM mode, a probe size of 0.1 nm at semi-convergence angle of 22 mrad was used for HAADF-STEM imaging. The HAADF detectors covered an angular range of 90–176 mrad. The magnetic hysteresis (M-H) loops were measured by a SQUID (Quantum Design, San Diego, CA, USA) with a magnetic field applied along the SrTiO₃ [100] and [001] directions, respectively. A quartz paddle and brass half-tube were used as sample holders for M-H loops along the in-plane (SrTiO₃ [100]) and out-of-plane (SrTiO₃ [001]) directions, respectively. The magnetic set-ups are shown in Figure S1 in the Supplementary Materials.

3. Results and Discussion

Figure 1a,b are low-magnification bright-field (BF) TEM images of LiFe₅O₈ thin films on SrTiO₃(001) substrates with thicknesses of 7.5 nm and 30 nm, respectively. The film–substrate interfaces are marked by horizontal arrows. The contrast variation within the

film can be discerned in both films. In Figure 1b, the oblique contrast lines shown by blue arrows are apparent. Figure 1c,d display the corresponding selected-area electron diffraction (SAED) pattern of the heterostructure in Figures 1a and 1b, respectively, recorded along the $[1\bar{1}0]$ zone axis of SrTiO_3 . In Figure 1c, apart from the diffraction spots of the SrTiO_3 substrate, denoted by a solid white rectangle, two sets of diffraction spots, denoted by a solid yellow rectangle and a dashed yellow rectangle, from the LiFe_5O_8 film can be distinguished, resulting in two film–substrate orientation relationships (ORs) represented by $[1\bar{1}0](001)_{\text{film}} // [1\bar{1}0](001)_{\text{substrate}}$ (cube-on-cube) and $[1\bar{1}0](111)_{\text{film}} // [1\bar{1}0](001)_{\text{substrate}}$. The $\text{SrTiO}_3(001)$ substrate surface has four-fold symmetry, which means the orthogonal $[110]$ and $[1\bar{1}0]$ directions are equivalent, while the $\text{LiFe}_5\text{O}_8(111)$ has three-fold symmetry, and the in-plane $[1\bar{1}0]$ direction is different from the vertical $[11\bar{2}]$ direction. Thus, there exists an equivalent OR with a 90° in-plane orientation in relation to the OR of $[1\bar{1}0](111)_{\text{film}} // [1\bar{1}0](001)_{\text{substrate}}$. In Figure 1d, the diffraction spot of the SrTiO_3 substrate is denoted by a solid white rectangle. The diffraction spot denoted by the solid blue rectangle has 70.5° rotation relative to the diffraction spot denoted by a dashed blue rectangle, which results from the formation of twin domains. From the SAED results of these two films, the crystalline orientation domains form a 7.5 nm thick film; in contrast, there is only the presence of some $\{111\}$ TBs and an absence of crystalline orientation domains in the 30 nm thick film. Taking the lattice parameter of the SrTiO_3 substrate (0.3905 nm) as the calibration standard [28], the in-plane and out-of-plane lattice parameters of the 7.5 nm thick film are calculated to be 0.8319 nm and 0.8353 nm, respectively. Similarly, the in-plane and out-of-plane lattice parameters of the 30 nm thick film are calculated to be 0.8301 nm and 0.8359 nm, respectively. All the parameters are close to that of the bulk material (the lattice parameter of bulk LiFe_5O_8 is 8.290 nm [5]), indicating that the considerable mismatch in the strains of both films is relaxed, leaving low compressive strain in the film [10].

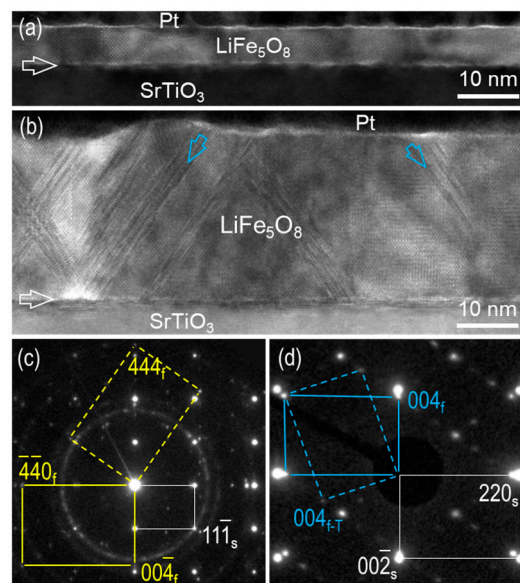


Figure 1. (a,b) Low-magnification BF-TEM images and (c,d) the corresponding SAED patterns of 7.5 nm thick and 30 nm thick LiFe_5O_8 films prepared on $\text{SrTiO}_3(001)$ substrate, recorded along the $[1\bar{1}0]$ SrTiO_3 zone axis. The film–substrate interface is indicated by horizontal arrows. The twin boundary is denoted by oblique blue arrows.

In order to further investigate the microstructure and strain relaxation behaviors, high-resolution HAADF-STEM experiments were performed. Figure 2a–c present atomic-resolution HAADF-STEM images showing the interfaces of the 7.5 nm thick film, viewed along the $[1\bar{1}0]$ zone axis of the SrTiO_3 substrate. Misfit dislocations form at the interface in both heterostructures. For the grain with the cube-on-cube OR (Figure 2a), the projected Burgers vector of misfit dislocations can be determined as $(a_f/4)[110]$ (a_f is the lattice

parameter of LiFe_5O_8). For the $[\bar{1}\bar{1}0](111)_{\text{film}} // [\bar{1}\bar{1}0](001)_{\text{substrate}}$ OR, misfit dislocations occur at the interfaces, as shown in Figure 2b,c. The projected Burgers vectors are determined to be $(a_f/8)[112]$ and $(a_f/4)[\bar{1}\bar{1}0]$, respectively. In contrast, for the heterostructure of the 30 nm thick film on the $\text{SrTiO}_3(001)$ substrate, a number of $\{111\}$ TBs, denoted by a blue arrow, appear within the LiFe_5O_8 film, as demonstrated in Figure 2d. $\{111\}$ TBs are common planar defects in spinel structures [7]. It should be noted that abnormal contrast was not observed in any HAADF images, indicating that there is no chemical segregation in the film.

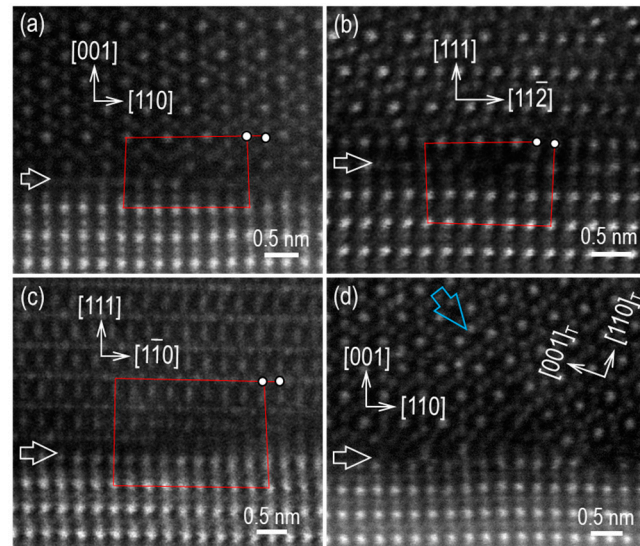


Figure 2. (a–d) High-resolution HAADF-STEM images of the heterostructures, viewed along the $[\bar{1}\bar{1}0]$ SrTiO_3 zone axis, showing the formation of misfit dislocations in differently oriented domains and twin boundaries (indicated by a blue arrow) in LiFe_5O_8 film. The film–substrate interfaces are denoted by horizontal white arrows.

Additionally, for the heterostructure of the 7.5 nm thick film prepared on the $\text{SrTiO}_3(001)$ substrate, the occurrence of two types of film–substrate ORs would form a columnar grain structure in the film. The coalescence of these grains inevitably leads to the formation of grain boundaries (GBs). Figure 3a–c present HAADF-STEM images containing such GBs. The boundaries appear curved through the film, as denoted by white dashed lines. It should be emphasized that there is no secondary phase or obvious element segregation at the boundaries.

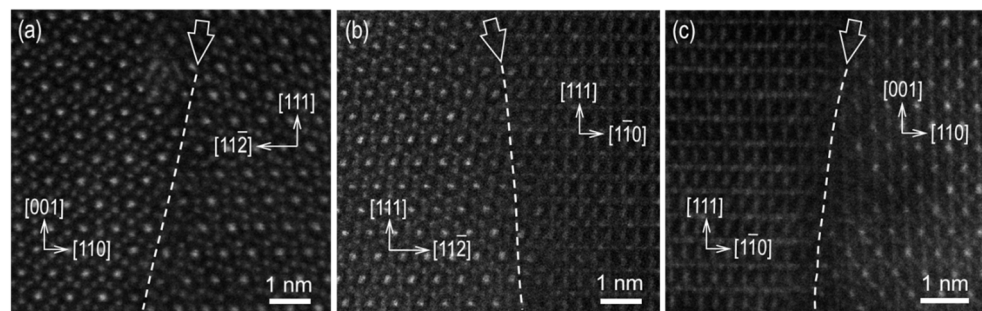


Figure 3. (a–c) HAADF-STEM images of grain boundaries in 7.5 nm thick film. The boundaries are denoted by white dashed lines and oblique white arrows.

Bulk LiFe_5O_8 (space group $Fd\bar{3}m$) and SrTiO_3 (space group $Pm\bar{3}m$) both have cubic structures. The lattice constant of bulk LiFe_5O_8 ($a_f = 0.8290$ nm) is approximately twice that of SrTiO_3 ($a_s = 0.3905$ nm), resulting in a one-unit cell length of LiFe_5O_8 , matching

the two-unit cell length of SrTiO₃ at the heterointerface, with a cube-on-cube epitaxy. Thus, the mismatch can be described as $[(a_f - 2a_s)/2a_s] \times 100\%$ [10], and the lattice mismatch is calculated to be about +6.2%. For the LiFe₅O₈(111)/SrTiO₃(001) epitaxy, the lattice mismatch along the [110]_f direction is the same as that of the cube-on-cube epitaxy, whereas the film–substrate lattice mismatch along the [112]_f direction is much larger. Based on the TEM results, different strain relaxation behaviors occur in the LiFe₅O₈ films through different defect configurations [29,30]. The appearance of oriented grains and misfit dislocations releases the compressive strain in the 7.5 nm thick film on the SrTiO₃ substrate. In contrast, the formation of a high density of twins within the film (denoted by the blue arrows in Figures 1b and 2d) mainly contributes to strain relaxation in the 30 nm thick film.

The magnetic properties of the LiFe₅O₈ films were characterized by the magnetic hysteresis loops using the SQUID system. The effect of the pure SrTiO₃ substrate was carefully eliminated. Figure 4a,b present the M-H hysteresis loops measured along the in-plane and out-of-plane directions of the 7.5 nm and 30 nm thick films separately. The in-plane saturation magnetization (M_s) of the 7.5 nm thick film is about 583 emu/cc, and the out-of-plane M_s is 465 emu/cc (experimental error for the magnetization (± 1 emu/cc)). Both values are significantly higher than that of bulk LiFe₅O₈ (2.5 μ B/formula unit ~ 320 emu/cc) [5]. The in-plane and the out-of-plane M_s of the 30 nm thick film are about 204 emu/cc and 154 emu/cc, respectively. The 7.5 nm thick film exhibits considerably higher M_s compared with the values in the literature (see Table S1 in Supplementary Materials). The insets in Figure 4a,b are the corresponding magnified hysteresis loops of the 7.5 nm thick film and 30 nm thick film from -400 Oe to 400 Oe, respectively. The in-plane and out-of-plane coercive fields (H_c) of the 7.5 nm thick film are about 65 Oe and 140 Oe, respectively, which are smaller than those of the 30 nm thick film (215 Oe and 166 Oe) (experimental error for coercivity values (± 10 Oe)). The magnetic parameters of the two films along the in-plane and out-of-plane directions are listed in Table S2 (see Supplementary Materials). The effective magnetic anisotropy coefficients K_{eff} of both films are calculated to be positive values [31]. Our SQUID measurement results show the apparent effect of film thickness on the M_s and H_c of LiFe₅O₈ thin films prepared on SrTiO₃(001) substrates.

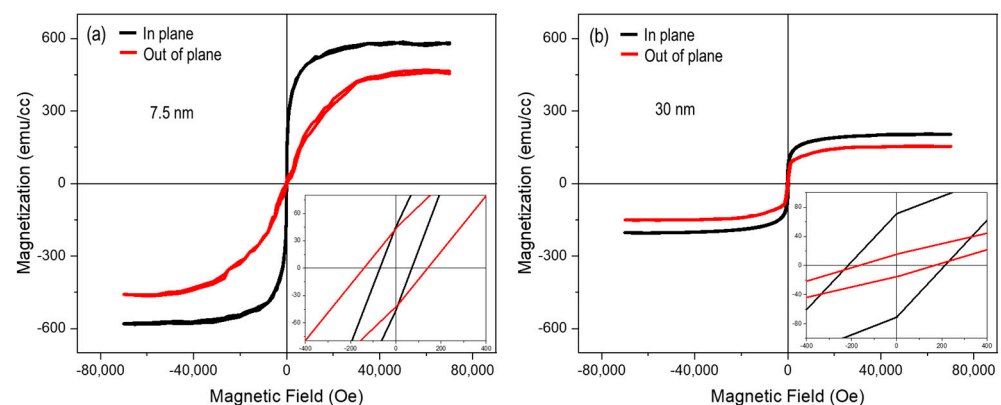


Figure 4. (a,b) In-plane and out-of-plane magnetic hysteresis loops of LiFe₅O₈ films with different thicknesses measured at room temperature (300 K). Inserts show the small-scale magnetic field from -400 Oe to 400 Oe loops.

It can be seen that the 7.5 nm thick film displayed higher saturation magnetization and a relatively lower coercive field in comparison with the 30 nm thick film. In fact, an enhancement in the magnetization and a decrease in the coercive field has been reported in thinner spinel films, e.g., NiFe₂O₄ and CoFe₂O₄ [21–23] and LiFe₅O₈ on MgAl₂O₄ substrates [10]. The anomalous cation distribution among the tetrahedral and octahedral sites of spinel structures has been thought to account for this phenomenon [14,21], and the partial presence of deficient rocksalt-like structures is assumed to be responsible for the

enhanced magnetization [32]. However, in our LiFe_5O_8 thin films, no chemical modulation or second phase was observed during the TEM investigations, ruling out anomalous Fe^{3+} distribution and the formation of rocksalt as the origins of the enhanced M_s . Thus, the most likely factors responsible for the difference in magnetic properties are the strain state and the microstructure of the film under the current magnetron deposition conditions. It is considered that the enhanced M_s in the 7.5 nm thick film is due to the distinct column grain structure and the possible oxygen vacancies at the GBs. The presence of oxygen vacancies is associated with reduced ions Fe^{2+} , which can mitigate the antiparallel-aligned spin of Fe^{3+} at tetrahedral sites and octahedral sites, resulting in enhancement of the net magnetic moment [1,33]. In contrast, the appearance of a high density of TBs with antiferromagnetic coupling [7] in the 30 nm thick film will weaken the M_s of the film [34]. The in-plane and out-of-plane H_c of the 30 nm thick film are higher than those of 7.5 nm thick film. The occurrence of antiferromagnetic defects and the effect of magnetic domain wall pinning induced by those defects are likely to make it difficult to turn over the magnetic domain during the magnetization process, which leads to a larger coercive field in the 30 nm thick film.

LiFe_5O_8 is a negative magnetostrictive material with saturation magnetostriction of ~ 27.8 ppm [10]. Compressive strain favors the in-plane orientation of magnetization [23,35]. Although strain relaxations occur in our LiFe_5O_8 films, tetragonal lattice distortions appear in both films under compressive strain, resulting in anisotropic magnetization in both films, as shown in Figure 4a,b. Also, the positive K_{eff} of both films indicates that both films have in-plane magnetic anisotropy [31]. Overall, varying thicknesses of the LiFe_5O_8 films on the $\text{SrTiO}_3(001)$ substrate can effectively modify the microstructural and magnetic properties of the films. High-resolution annular bright-field imaging to verify the presence of oxygen vacancies at GBs and theoretical calculations of magnetic coupling across the GBs can be further conducted in future investigations to elucidate the possible origin of enhanced M_s .

4. Conclusions

Epitaxial LiFe_5O_8 thin films with thicknesses of 7.5 nm and 30 nm were grown on a $\text{SrTiO}_3(001)$ substrate. Microstructural investigations show that $(111)_{\text{film}}// (001)_{\text{substrate}}$ and $(001)_{\text{film}}// (001)_{\text{substrate}}$ ORs appear in the 7.5 nm thick film, and TBs occur in the 30 nm thick film, respectively, which contributes to lattice misfit strain. Importantly, the 7.5 nm thick film displays higher saturation magnetization and a relatively lower coercive field in comparison with the 30 nm thick film. The appearance of GBs and the absence of TBs in the 7.5 nm thick film are probably responsible for the enhanced M_s . Our results demonstrate that changing the film thickness could effectively tune the microstructure and magnetic properties in epitaxial LiFe_5O_8 thin films.

Supplementary Materials: The following supporting information can be downloaded at: <https://www.mdpi.com/article/10.3390/coatings13122097/s1>, Figure S1: magnetic set-up for (a) in-plane (IP) and (b) out-of-plane SQUID measurements; Table S1: saturation magnetization (M_s) of LiFe_5O_8 films with different thicknesses grown on different substrates in the literatures; Table S2: in-plane (IP) and out-of-plane (OP) magnetic parameters of 7.5 nm thick film and 30 nm thick film. Reference [36] is cited in the Supplementary Materials.

Author Contributions: Conceptualization, K.L.; investigation, K.L. and R.Z.; writing—original draft preparation, K.L.; writing—review and editing, L.L., J.L. and S.Z.; supervision, L.L. All authors have read and agreed to the published version of the manuscript. All authors have read and agreed to the published version of the manuscript.

Funding: This research was funded by the Guangdong Major Project of Basic and Applied Basic Research (No. 2021B0301030003), the Science and Technology Planning Project of Suzhou City (No. SZS2022015), the Natural Science Foundation of the Jiangsu Higher Education Institutions of China (Grant: 21KJB510022), and the Cultivation project of Suzhou vocational University (SVU2021py02).

Institutional Review Board Statement: Not applicable.

Informed Consent Statement: Not applicable.

Data Availability Statement: Data are contained within the article and supplementary materials.

Acknowledgments: We thank the Suzhou Key Laboratory of Smart Energy Technology for their support with the experiments of characterization.

Conflicts of Interest: The authors declare no conflict of interest.

References

1. White, G.O.; Patton, C.E. Magnetic Properties of Lithium Ferrite Microwave Materials. *J. Magn. Magn. Mater.* **1978**, *9*, 299–317. [[CrossRef](#)]
2. Sugimoto, M. The Past, Present, and Future of Ferrites. *J. Am. Ceram. Soc.* **1999**, *82*, 269–280. [[CrossRef](#)]
3. Lüders, U.; Barthélémy, A.; Bibes, M.; Bouzehouane, K.; Fusil, S.; Jacquet, E.; Contour, J.-P.; Bobo, J.-F.; Fontcuberta, J.-F.; Fert, A. NiFe₂O₄: A Versatile Spinel Material Brings New Opportunities for Spintronics. *Adv. Mater.* **2006**, *18*, 1733–1736. [[CrossRef](#)]
4. Suzuki, Y. Epitaxial Spinel Ferrite Thin Films. *Annu. Rev. Mater. Res.* **2001**, *31*, 265–289. [[CrossRef](#)]
5. Boyraz, C.; Mazumdar, D.; Iliev, M.; Marinova, V.; Ma, J.; Srinivasan, G.; Gupta, A. Structural and magnetic properties of lithium ferrite (LiFe₅O₈) thin films: Influence of substrate on the octahedral site order. *Appl. Phys. Lett.* **2011**, *98*, 012507. [[CrossRef](#)]
6. Wei, J.D.; Knittel, I.; Hartmann, U.; Zhou, Y.; Murphy, S.; Shvets, I.V.; Parker, F.T. Influence of the Antiphase Domain Distribution on the Magnetic Structure of Magnetite Thin Films. *Appl. Phys. Lett.* **2006**, *89*, 122517. [[CrossRef](#)]
7. Chen, C.L.; Li, H.P.; Seki, T.; Yin, D.Q.; Sanchez-Santolino, G.; Inoue, K.; Shibata, N.; Ikuhara, Y. Direct Determination of Atomic Structure and Magnetic Coupling of Magnetite Twin Boundaries. *ACS Nano* **2018**, *12*, 2662–2668. [[CrossRef](#)]
8. Udhayakumar, S.; Kumar, G.J.; Kumar, E.S.; Navaneethan, M.; Kamala Bharathi, K. Electrical, Electronic and Magnetic Property Correlation Via Oxygen Vacancy Filling and Scaling-law Analysis in LiFe₅O₈ Thin Films Prepared by Pulsed Laser Deposition. *J. Mater. Chem. C* **2022**, *10*, 15051–15060. [[CrossRef](#)]
9. Liu, X.; Wu, M.; Qu, K.; Gao, P.; Mi, W. Atomic-Scale Mechanism of Grain Boundary Effects on the Magnetic and Transport Properties of Fe₃O₄ Bicrystal Films. *ACS Appl. Mater. Inter.* **2021**, *13*, 6889–6896. [[CrossRef](#)]
10. Zhang, R.; Liu, M.; Lu, L.; Mi, S.B.; Wang, H. Strain-tunable magnetic properties of epitaxial lithium ferrite thin film on MgAl₂O₄ substrates. *J. Mater. Chem. C* **2015**, *3*, 5598–5602. [[CrossRef](#)]
11. Hu, G.; Choi, J.H.; Eom, C.B.; Harris, V.G.; Suzuki, Y. Structural Tuning of the Magnetic Behavior in Spinel-Structure Ferrite Thin Films. *Phys. Rev. B* **2000**, *62*, R779–R782. [[CrossRef](#)]
12. Uusi-Esko, K.; Rautama, E.-L.; Laitinen, M.; Sajavaara, T.; Karppinen, M. Control of Oxygen Nonstoichiometry and Magnetic Property of MnCo₂O₄ Thin Films Grown by Atomic Layer Deposition. *Chem. Mater.* **2010**, *22*, 6297–6300. [[CrossRef](#)]
13. Foerster, M.; Rebled, J.M.; Estradé, S.; Sánchez, F.; Peiró, F.; Fontcuberta, J. Distinct Magnetism in Ultrathin Epitaxial NiFe₂O₄ Films on MgAl₂O₄ and SrTiO₃ Single Crystalline Substrates. *Phys. Rev. B* **2011**, *84*, 144422. [[CrossRef](#)]
14. Gao, C.Y.; Cao, C.M.; Zhao, J.Z. Structure and Magnetic Properties of Epitaxial LiFe₅O₈ Film with Different Growth Temperature. *Appl. Phys. A* **2019**, *125*, 566. [[CrossRef](#)]
15. Rigato, F.; Estradé, S.; Arbiol, J.; Peiró, F.; Lüders, U.; Martí, X.; Sánchez, F.; Fontcuberta, J. Strain-induced stabilization of new magnetic spinel structures in epitaxial oxide heterostructures. *Mater. Sci. Eng. B* **2007**, *144*, 43–48. [[CrossRef](#)]
16. Praus, R.B.; Leibold, B.; Gross, G.M.; Habermeier, H.U. Thickness dependent properties of La_{0.67}Ca_{0.33}MnO₃ thin films. *Appl. Surf. Sci.* **1999**, *138–139*, 40–43. [[CrossRef](#)]
17. Matvejeff, M.; Lippmaa, M. Growth of InFeCoO₄ thin films on SrTiO₃ and MgO substrates. *J. Cryst. Growth* **2010**, *312*, 2386–2392. [[CrossRef](#)]
18. Wang, Y.; Li, D.F.; Dai, J.Y. Microstructure and magnetic properties of a novel spinel (Zn,Co)Fe₂O₄ thin film on the SrTiO₃ substrate. *J. Cryst. Growth* **2010**, *313*, 26–29. [[CrossRef](#)]
19. Moussy, J.B.; Gota, S.; Bataille, A.; Guittet, M.J.; Gautier-Soyer, M.; Delille, F.; Diény, B.; Ott, F.; Doan, T.; Warin, P.; et al. Thickness dependence of anomalous magnetic behavior in epitaxial Fe₃O₄ thin films: Effect of density of antiphase boundaries. *Phys. Rev. B* **2004**, *70*, 174448. [[CrossRef](#)]
20. Mi, S.B.; Zhang, R.Y.; Lu, L.; Liu, M.; Wang, H.; Jia, C.L. Atomic-scale structure and formation of antiphase boundaries in α -Li_{0.5}Fe_{2.5}O₄ thin films on MgAl₂O₄ substrates. *Acta Mater.* **2017**, *127*, 178–184. [[CrossRef](#)]
21. Gao, C.; Jiang, Y.; Yao, T.; Tao, A.; Yan, X.; Li, X.; Chen, C.; Ma, X.L.; Ye, H. Atomic Origin of Magnetic Coupling of Antiphase Boundaries in Magnetite Thin Films. *J. Mater. Sci. Technol.* **2022**, *107*, 92–99. [[CrossRef](#)]
22. Lüders, U.; Bibes, M.; Bobo, J.-F.; Cantoni, M.; Bertacco, R.; Fontcuberta, J. Enhanced Magnetic Moment and Conductive Behavior in NiFe₂O₄ Spinel Ultrathin Film. *Phys. Rev. B* **2005**, *71*, 134419. [[CrossRef](#)]
23. Gatel, C.; Warot-Fonrose, B.; Matzen, S.; Moussy, J.B. Magnetism of CoFe₂O₄ Ultrathin Films on MgAl₂O₄ Driven by Epitaxial Strain. *Appl. Phys. Lett.* **2013**, *103*, 092405. [[CrossRef](#)]
24. Hoppe, M.; Döring, S.; Gorgoi, M.; Cramm, S.; Müller, M. Enhanced Ferrimagnetism in Auxetic NiFe₂O₄ in the Crossover to the Ultrathin-Film Limit. *Phys. Rev. B* **2015**, *91*, 054418. [[CrossRef](#)]
25. Du, K.F.; Zhang, C.B.; Ma, Y.S.; Wang, P.L.; Yu, R.; Li, W.M.; Zheng, K.Y.; Cheng, X.H.; Tang, D.Y.; Deng, B.W.; et al. An Iron-base Oxygen-Evolution Electrode for High-temperature Electrolyzers. *Nat. Commun.* **2023**, *14*, 253. [[CrossRef](#)]

26. Hu, Y.Z. α -LiFe₅O₈: A Promising Iron-Based Anode Material for Lithium-ion Batteries. *Mater. Sci. Eng. B* **2023**, *297*, 116792. [[CrossRef](#)]
27. Subash, S.; Udhayakumar, S.; Kumaresan, L.; Patro, L.N.; Kumaran, V.; Senthil Kumar, E.; Navaneethan, M.; Kyung Kim, D.; Kamala Bharathi, K. Ordered LiFe₅O₈ Thin Films Prepared by Pulsed Laser Deposition as an Anode Material for All-solid Thin Film Batteries. *Electrochim. Acta* **2023**, *454*, 142318. [[CrossRef](#)]
28. Howard, S.A.; Yau, J.K.; Anderson, H.U. Structural Characteristics of Sr_{1-x}La_xTi_{3+δ} as a Function of Oxygen Partial Pressure at 1400 °C. *J. Appl. Phys.* **1989**, *65*, 1492–1498. [[CrossRef](#)]
29. Jain, S.C.; Harker, A.H.; Cowley, R.A. Misfit Strain and Misfit Dislocations in Lattice Mismatched Epitaxial Layers and Other Systems. *Philos. Mag. A* **1997**, *75*, 1461–1515. [[CrossRef](#)]
30. Regmi, S.; Li, Z.; Srivastava, A.; Mahat, R.; Shambhu, K.C.; Rastogi, A.; Galazka, Z.; Datta, R.; Mewes, T.; Gupta, A. Structural and Magnetic Properties of NiFe₂O₄ Thin Films Grown on Isostructural Lattice-matched Substrates. *Appl. Phys. Lett.* **2021**, *118*, 152402. [[CrossRef](#)]
31. Salaheldeen, M.; Martínez-Goyeneche, L.; Álvarez-Alonso, P.; Fernández, A. Enhancement the Perpendicular Magnetic Anisotropy of Nanopatterned Hard/soft Bilayer Magnetic Antidot Arrays for Spintronic Application. *Nanotechnology* **2020**, *31*, 485708. [[CrossRef](#)] [[PubMed](#)]
32. Rodewald, J.; Thien, J.; Ruwisch, K.; Bertram, F.; Kuepper, K.; Wollschläge, J. Enhanced magnetization of ultrathin NiFe₂O₄ films on SrTiO₃ related to cation disorder and anomalous strain. *Phys. Rev. Mater.* **2020**, *4*, 064404. [[CrossRef](#)]
33. Zhang, J.; Liu, W.; Zhang, M.; Zhang, X.; Niu, W.; Gao, M.; Wang, X.; Du, J.; Zhang, R.; Xu, Y. Oxygen pressure-tuned epitaxy and magnetic properties of magnetite thin films. *J. Magn. Magn. Mater.* **2017**, *432*, 472–476. [[CrossRef](#)]
34. Liu, K.; Zhang, R.Y.; Lu, L.; Mi, S.B.; Liu, M.; Wang, H.; Wu, S.Q.; Jia, C.L. Atomic-Scale Investigation of Spinel LiFe₅O₈ Thin Films on SrTiO₃ (001) Substrates. *J. Mater. Sci. Technol.* **2020**, *40*, 31–38. [[CrossRef](#)]
35. Fritsch, D.; Ederer, C. Epitaxial Strain Effects in the Spinel Ferrites CoFe₂O₄ and NiFe₂O₄ from First Principles. *Phys. Rev. B* **2010**, *82*, 104117. [[CrossRef](#)]
36. Yang, J.; Lei, J.F.; Du, K.; Zheng, X.D.; Jin, X.J. The Microwave Magnetism of Epitaxy LiFe₅O₈ Thin Film Modulated by Thickness. *Curr. Appl. Phys.* **2020**, *20*, 589–592.

Disclaimer/Publisher's Note: The statements, opinions and data contained in all publications are solely those of the individual author(s) and contributor(s) and not of MDPI and/or the editor(s). MDPI and/or the editor(s) disclaim responsibility for any injury to people or property resulting from any ideas, methods, instructions or products referred to in the content.